DISPERSION CURVES AND SYNTHETIC MICROSEISMOGRAMS IN UNBONDED CASED BOREHOLES

by

Kenneth M. Tubman, Stephen P. Cole*, C.H. Cheng and M.N. Toksöz

Earth Resources Laboratory
Department of Earth, Atmospheric, and Planetary Sciences
Massachusetts Institute of Technology
Cambridge, MA 02139

ABSTRACT

The dispersion relations and impulse response are calculated for a geometry consisting of an arbitrary number of coaxial annuli surrounding a central cylinder. The annuli may be either solid or fluid. The formulation allows any number of solid and fluid layers in any sequence. The only restrictions are that the central cylinder is fluid and the outermost layer is solid. A propagator matrix method is used to relate stresses and displacements across layer boundaries. Fluid layers are handled by directly relating the displacements and stresses across these layers.

A number of examples of dispersion curves and synthetic waveforms are given. The specific geometries used are those for a pipe not bonded to the cement and for the pipe well bonded to the cement but with the cement not bonded to the formation.

The addition of an intermediate fluid layer can have a large effect on the calculated waveforms. More surprisingly, this additional layer may have only minor effects, indicating possible difficulties in establishing its presence. If the fluid layer lies between the steel and the cement (free pipe situation), the first arrival is from the steel. This is the case even for a very thin layer, or microannulus. If the fluid layer is between the cement and the formation, the thicknesses of the cement and fluid layers become important in determining what will be the first arrival as well as the nature of the microseismogram.

An intermediate fluid layer is shown to have the additional effect of introducing another Stoneley wave mode. This mode has only a small amount of energy and so it does not contribute significantly to the calculated microseismograms.

INTRODUCTION

A number of studies have investigated wave propagation in radially layered boreholes (Baker, 1981; Cheng *et al.*, 1981; Schoenberg *et al.*, 1981; Chan and

---

*Now at Western Geophysical Co., Houston, TX.

Tsang, 1983; Chang and Everhart, 1983; Tubman *et al.*, 1984). While these
treatments are general, they all make the assumption that the annuli are all
solids. This restriction is lifted in this study. There are no limitations on the
placement and number of fluid layers except that the central cylinder must be
a fluid and the outer formation must be solid. The inclusion of fluid layers has
applications in modeling the situation of unbonded pipe and cement in cased
boreholes. Chang and Everhart (1983) modeled the free pipe situation by
allowing discontinuities in the axial displacement at the steel-cement interface
and requiring zero axial stress at this boundary. There was no additional fluid
layer in their formulation. The inclusion of a fluid layer allows the examination
of the effects of the thickness of the layer, rather than only the limiting case of
zero thickness.

THEORETICAL DEVELOPMENT

The model consists of a fluid cylinder surrounded by an arbitrary number
of coaxial annuli (Figure 1). The annuli can be solid, such as the casing or
cement; or fluid, such as drilling mud. The outermost, infinite layer is a solid.
Each layer is homogeneous and isotropic. Complex layer parameters are used
to incorporate attenuation into the calculations (Aki and Richards, 1980; Cheng
et al., 1982; Tubman *et al.*, 1984).

In layer n, the radial and axial displacements, u_n and v_n, are given by:

$$u_n = \frac{\partial \varphi_n}{\partial r} - \frac{\partial \psi_n}{\partial z} \tag{1a}$$

$$v_n = \frac{\partial \varphi_n}{\partial z} + \frac{\partial \left[r \psi_n \right]}{r \, \partial r} \tag{1b}$$

and the normal and tangential stresses σ_n and τ_n are given by:

$$\sigma_n = \rho_n \left(\frac{\nu_n}{1 - \nu_n} \right) \frac{\partial^2 \varphi_n}{\partial t^2} + 2\mu_n \left(\frac{\partial^2 \varphi_n}{\partial r^2} - \frac{\partial^2 \psi_n}{\partial r \, \partial z} \right) \tag{1c}$$

$$\tau_n = \rho_n \frac{\partial^2 \psi_n}{\partial t^2} + 2\mu_n \left(\frac{\partial^2 \varphi_n}{\partial r \, \partial z} - \frac{\partial^2 \psi_n}{\partial z^2} \right) \tag{1d}$$

where ρ_n, ν_n, and μ_n are the density, Poisson's ratio, and shear modulus for
layer n.

The scalar potential, φ_n, and azimuthal component of the vector potential
ψ_n, are given by:

$$\varphi_n = \left[A_n K_0(l_n r) + A'_n I_0(l_n r) \right] e^{ik(z - ct)} \tag{2a}$$

$$\psi_n = \left[B_n K_1(m_n r) + B'_n I_1(m_n r) \right] e^{ik(z - ct)} \tag{2b}$$

where I_0, I_1, K_0, and K_1 are modified Bessel functions of the first and second

kind. c is the phase velocity and z the source-receiver separation. k is the axial component of the wave number and l_n and m_n are the radial components of the P and S wave numbers. A_n, A'_n, B_n, and B'_n are constants for layer n.

Equations (1) can be written:

$$\mathbf{u}_n(r) = \mathbf{D}_n(r_n)(r)\mathbf{a}_n \tag{3}$$

where:

$$\mathbf{u}_n = \begin{bmatrix} u_n \\ v_n \\ \sigma_n \\ \tau_n \end{bmatrix} \tag{4}$$

and:

$$\mathbf{a}_n = \begin{bmatrix} A_n \\ A'_n \\ iB_n \\ iB'_n \end{bmatrix} \tag{5}$$

$\mathbf{D}_n(r_n)$ is a $4x4$ matrix whose terms are determined from substitution of equations (2) into equations (1). The elements of $\mathbf{D}_n(r_n)$ are given explicitly in Tubman *et al.* (1984).

It is necessary to relate the stresses and displacements in the outermost, infinite layer to those in the central fluid cylinder. In the case with all solid layers this expression is found to be (Tubman *et al.*, 1984):

$$\mathbf{u}_n(r_{N-1}) = \mathbf{D}_{N-1}(r_{N-1})\mathbf{D}_{N-1}^{-1}(r_{N-2})\mathbf{D}_{N-2}(r_{N-2})...\mathbf{D}_2^{-1}(r_1)\mathbf{u}_2(r_1) \tag{6}$$

which can be re-written as

$$\mathbf{Ga}_N = \mathbf{u}_2(r_1) \tag{7}$$

where:

$$\mathbf{G} = \mathbf{D}_N(r_{N-1})\mathbf{D}_{N-1}^{-1}(r_{N-1})\mathbf{D}_{N-1}(r_{N-2})...\mathbf{D}_2^{-1}(r_2)\mathbf{D}_2(r_1) \tag{8}$$

The same formulation is used between the infinite formation and the outermost fluid layer that is used when all the layers are solid. Equation (7) cannot be extended to relate the displacement-stress vector across all the layers because not all components of the displacement-stress vector are continuous at a solid-fluid boundary. At the outermost fluid layer, the boundary conditions change and so the displacements and stresses can not be related across the boundaries in the same manner as before. The normal displacement, u, and normal stress, σ, are continuous. The tangential stress, τ, vanishes at the boundary. The tangential displacement, v, is discontinuous because the solid and fluid are free to slip along the interface.

The G matrix we have now can relate the displacement-stress vector inward only until the outermost fluid layer (layer f). At that point the axial

displacement is no longer continuous. So we now have

$$\mathbf{G}\mathbf{a}_N = \mathbf{u}_{f+1}(r_f) \tag{9}$$

where r_f is the outer radius of layer f and $\mathbf{u}_{f+1}$ is the displacement-stress vector in layer $f+1$.

Inside layer f, each boundary must be handled individually to allow for general geometries. Starting at the center and working out to layer f, the constants for each layer n, $(\mathbf{a}_n)$, are written in terms of $\mathbf{a}_1$ (which is just A'_1). Each layer may be either solid or fluid. This requires checking at each boundary to see if the next layer is a fluid or a solid. The type of boundary determines which components of the displacement-stress vector are continuous. This process yields the displacements and stresses in layer f in terms of those in the central fluid layer. They are then matched to those in the next layer out (layer $f+1$). This completes the relationship from the infinite layer to the central cylinder.

Dispersion Relation

The displacements and stresses have been related from the central fluid cylinder to the outermost fluid layer, (layer f). Application of the above results yields A_f and A'_f in terms of A'_1. These are then used in equation (9) to complete the relation of the displacements and stresses from the central fluid cylinder to the outer, infinite formation.

Since there are no incoming waves in the outermost layer, $A'_N = B'_N = 0$. In addition, $A_1 = B_1 = 0$ so that the displacements and stresses remain finite at $r = 0$. $B'_1 = 0$ as well because there is no vector potential in a fluid. Equation (9) is thus reduced to:

$$\begin{vmatrix} u_f(r_f) & -G_{11} & -G_{13} \\ \sigma_f(r_f) & -G_{31} & -G_{33} \\ 0 & G_{41} & G_{43} \end{vmatrix} \begin{bmatrix} A'_1 \\ A_N \\ B_N \end{bmatrix} = 0 \tag{10}$$

This is the period equation for wave propagation in a borehole with a mixture of solid and fluid radial layers. Values of k and c for which this equation is satisfied yield the phase velocity dispersion relations.

Synthetic Microseismograms

In order to generate synthetic microseismograms it is necessary to include a source into the calculations. This is accomplished by imposing a boundary condition at r_1, the interface between the central fluid layer and the first annulus. The condition specified is an expression for a $K_0(l_1 r)$ source in the frequency-wavenumber domain (Cheng *et al.*, 1982; Tubman *et al.*, 1984). This represents a point isotropic source on the borehole axis. The above calculations are then repeated in order to derive a relation similar to equation (10). This relation is used to solve for A'_1 which is then substituted into the form for the pressure response. In the time domain the pressure response, P, inside the borehole is : (Tsang and Rader, 1979; Cheng *et al.*, 1982; Tubman *et al.*, 1984):

$$P(r,z,t) = \int\limits_{-\infty}^{\infty} X(\omega)e^{-i\omega t}d\omega \int\limits_{-\infty}^{\infty} A'_1 I_0(l_1 r)e^{ikz} dk \qquad (11)$$

$P(r,z,t)$ is the pressure response, z the source-receiver separation, t time, and $X(\omega)$ the source spectrum. A'_1 is the only non-zero constant associated with the potentials in the central fluid cylinder. The excitation resulting from the $K_0(l_1 r)$ source is added to the response function to give the total pressure field.

NUMERICAL EXAMPLES

The geometries considered here have an intermediate fluid layer placed in one of two commonly occurring locations. The first is between the pipe and the cement. This models the case of no pipe-cement bonding, or free pipe. The other geometry represents the case of poor cement-formation bonding. This is represented through the inclusion of a fluid layer between the cement and the formation.

Figure 2 shows a number of microseismograms for the free pipe situation. All microseismograms are for the same source-receiver separation, 10 ft., and source, centered at 13 kHz. The source is the same as that used by Tubman *et al.*, (1984). The formation velocities are 13.12 ft/ms for V_p and 7.0 ft/ms for V_s. The difference in the microseismograms of Figure 2 is the thickness of the fluid layer between the steel and the cement. The distance between the steel and the formation remains constant, so the cement thickness decreases as the fluid thickness increases. The fluid is replacing cement. The first microseismogram in Figure 2 has no fluid layer. This is the well bonded situation. The last waveform has no cement layer. The layers are just ones of fluid, steel, fluid, and the formation. Between these two extremes the thickness of the fluid layer increases in .25 inch increments (and the thickness of the cement layer decreases by this amount).

There is a large change in the character of the waveforms when the fluid layer in introduced. The microseismogram for the well bonded situation displays clear formation P wave and S wave arrivals. There is no distinct casing arrival. The additional fluid layer frees the pipe so the casing arrival is very obvious. The ringing from the steel completely obscures the formation arrival. Little change occurs in the waveforms as the thickness of the fluid layer increases. The casing arrival dominates throughout, although a slight increase in the amplitude and duration of this pipe signal may be observed as the fluid layer becomes larger.

Even a very thin fluid layer produces similar results. Tubman *et al.* (this report) show an example where the thickness of the fluid layer has been reduced to .001 inches in order to model a microannulus. The first arrival is from the casing despite the very small thickness of the fluid layer. Chang and Everhart (1983) showed the same ringing even at the limit of zero fluid thickness.

The important factor in determining the first arrival is whether or not the pipe is bonded to the cement. The thickness of the fluid layer between the steel and the cement has only a minor influence on the character of the observed time series.

Dispersion curves corresponding to some of the microseismograms of Figure 2 are shown in Figures 3 to 6. The first one, Figure 3, gives the phase velocity dispersion relations for the well bonded cased hole situation. There are three distinct modes in the frequency range shown: the Stoneley and two for the pseudo-Rayleigh waves. (Only a small portion of the second pseudo-Rayleigh mode is seen.) The Stoneley wave is only slightly dispersive and is not cut off at low frequencies. The pseudo-Rayleigh curves are much more dispersive and are cut off at the shear velocity of the formation.

A fluid layer of thickness .25 inches has been inserted between the steel and the cement in Figure 4. As before, the thickness of the cement is .25 inches less. The pseudo-Rayleigh curves are shifted to lower frequencies than in the well bonded situation. The extra fluid layer could be causing an effect similar to that produced by an increase in the borehole effective radius (Cheng and Toksöz, 1981). The Stoneley velocity is slightly lower at higher frequencies but the curve has not changed substantially. The interesting thing to note in Figure 4 is the presence of an additional Stoneley mode. This additional mode is due to the presence of the intermediate fluid layer between the steel and the cement. This mode has significantly lower velocity and is more dispersive than the one which was also observed in the well bonded situation.

In Figure 5 the thickness of the fluid layer is increased to 1.5 inches. The pseudo-Rayleigh curves have moved to still lower frequencies but the general shape of the curves has not changed. The first Stoneley mode has lower velocities in a small region about 20 kHz but the shift is not significant. The second Stoneley mode has moved to much higher velocities. The Stoneley modes are now almost identical to those that observed in the case of no cement layer (Figure 6.)

The fluid layer has been decreased in thickness in Figure 7. This is the model of a microannulus. The fluid layer has a thickness of only .001 inches. The pseudo-Rayleigh velocities have shifted back slightly to higher frequencies. The first Stoneley mode shows minor changes but the additional mode is now gone. The fluid layer is now too thin to allow the propagation of the addition mode.

It is important to note that this additional Stoneley mode has not been observed in the microseismograms. This can be understood by looking at the frequency-wavenumber information (Figure 8). The arrival in question is the first encountered (counter-clockwise) from the kr axis. Clearly, there is very little energy associated with this wave. The power is not sufficient to be observable in the time domain. The fastest two arrivals are casing modes which were also observed by Chang and Everhart (1983).

Figure 9 is the same as Figure 2 except that the intermediate fluid layer is now located between the cement and the formation. Th first microseismogram has no intermediate fluid layer and the last has no cement layer. (These are the same waveforms shown in Figure 2.) Here it is clear that the character of the waveform changes as the thicknesses of the fluid and cement layers change. With the thick cement layer and thin fluid layer the formation arrival can still be distinguished. At the other extreme, with a thin cement layer and a thick fluid layer, the waveform has basically the same appearance as that in the free pipe situation. The first arrival varies as the amount of cement bonded to

the steel varies. This first arrival appears to be a signal due to the combination of the steel and the cement. A larger amount of cement damps out the ringing of the pipe decreasing the amplitude and duration of the first arrival. This same relationship between cement thickness and casing signal amplitude was observed by Walker (1968) in data from test wells with controlled bonding situations. The cement is also much slower than the steel, so increased influence on the velocity of the first arrival (due to the greater thickness) results in a lower velocity. It should be noted that while the change in velocity of the first arrival is fairly clear in Figure 9, the cement velocity used is much less than the velocity of the steel. If the cement was faster, the change in velocity could be much less. The cement only influences the velocity of the first arrival to be less than that of the steel. The steel velocity still is the dominant factor.

A thick cement layer bonded to the pipe is not sufficient to ensure that the formation arrival will be clear and distinct. Figures 10 and 11 have the same amount of cement (1.6875 inches) bonded to the pipe. The fluid layers are of different thicknesses though. The hole radius is larger in Figure 11 so that the fluid layer thickness is 1.25 inches compared with .0625 inches in Figure 10. While the formation signal is small in Figure 10, it is clear and able to be distinguished. The first arrival in Figure 11 is more obscure and difficult to identify.

Figures 12 to 14 show similar behavior for the dispersion curves as in the free pipe situation. A thicker intermediate fluid layer shifts the pseudo-Rayleigh dispersion curves to lower frequencies relative to the thin layer (Figures 12 and 13). The primary Stoneley mode changes only slightly and the additional Stoneley mode has significantly higher velocity with the thicker fluid layer. Again, the second Stoneley mode disappears completely when the thickness of the fluid layer is very small (Figure 14). A thick fluid layer yields curves that are virtually the same as those with no cement layer. Much more study is warranted on the nature of this additional Stoneley mode.

CONCLUSIONS

A formulation has been developed for the phase velocity dispersion relations and impulse response of radially layered cylindrical geometries including intermediate fluid layers. Examples are given for a number of situations encountered in poorly bonded cased boreholes. It is found that in the case of a free pipe, (with a fluid layer between the steel and the cement), the presence of the fluid layer is the most important factor in determining the nature of the microseismogram and what will be the first arrival. The thickness of the layer has only minor effects. If there is good pipe-cement bond but no cement-formation bond the thickness of the fluid layer as well as that of the cement layer become important. A thick layer of cement bonded to the steel can damp out the ringing of the casing arrival making it possible to identify the formation arrivals. If the cement layer is thinner, the first arrival will be from a combination of the steel and the cement.

A second Stoneley mode is shown to exist in the presence of an intermediate fluid layer of sufficient thickness. The nature of this wave is most dependent upon the parameters of the fluid layer. The additional Stoneley

mode is found to have only a small amount of energy and so does not contribute significantly to observed microseismograms. More study is required to fully understand the propagation of this additional mode.

REFERENCES

Aki, K. and Richards, P., 1980, Quantitative Seismology Theory and Methods: v.I., San Francisco, W.H. Freeman and Co.

Baker, L.J., 1981, The effect of the invaded zone in full waveform acoustic logging: 51st Annual International SEG Meeting, Los Angeles, CA.

Chan, A.K. and Tsang, L., 1983, Propagation of acoustic waves in a fluid-filled borehole surrounded by a concentrically layered transversely isotropic formation: J. Acoust. Soc. Am., 74, 1605-1616

Chang, S.K. and Everhart, A.H., 1983, A study of sonic logging in a cased borehole: J. Pet. Tech., v.35., p.1745-1750.

Cheng, C.H. and Toksöz, M.N., 1981, Elastic wave propagation in a fluid-filled borehole and synthetic acoustic logs: Geophysics, v.46., p.1042-1053.

Cheng, C.H., Tubman, K.M., and Toksöz, M.N., 1981, Propagation of seismic waves in a multilayered borehole: 51st Annual International SEG Meeting, Los Angeles, CA.

Cheng, C.H., Toksöz, M.N., and Willis, M.E., 1982, Determination of in situ attenuation from full waveform acoustic logs: J. Geophys. Res., v.87., p.5477-5484.

Cole, S.P., 1983, Guided wave dispersion in a borehole containing multiple fluid layers, B.S. Thesis, Department of Physics, Massachusetts Institute of Technology, Cambridge, MA.

Schoenberg, M., Marzetta, T., Aron, J., and Porter, R., 1981, Space-time dependence of acoustic waves in a borehole: J. Acoust. Soc. Am., v.70., p.1496-1507.

Tubman, K.M., Cheng, C.H., and Toksöz, M.N., 1984, Synthetic full waveform acoustic logs in cased boreholes: Geophysics, in press.

Walker, T., 1968, A full-wave display of acoustic signal in cased holes: J. Pet. Tech., p.818-824.

APPENDIX

This appendix gives the details of the calculations for each type of interface. The constants A_n, A'_n, B_n and B'_n are found in terms of the constants in the next layer inward (layer $n-1$). These are in turn expressed in terms of A'_1 and possibly A_n from an inner layer. These are the constants that determine the potentials for the layers. The relationships between these terms are expressed using two sets of constants: a_i and c_i. These constants have no particular physical meaning. They are used only to keep the derived expressions manageable. The results of each of the following sections can be used as the starting point for another section if further calculations are required.

Fluid-Solid Boundary

Let layer n be the fluid layer and layer $n+1$ the solid. The boundary is then at r_n. The boundary conditions are continuity of radial displacement and stress and zero axial stress. The axial displacement can be discontinuous.

$$u_n(r_n) = u_{n+1}(r_n) \tag{A1a}$$

$$\sigma_n(r_n) = \sigma_{n+1}(r_n) \tag{A1b}$$

$$\tau_n(r_n) = \tau_{n+1}(r_n) = 0 \tag{A1c}$$

In the fluid layer there are two constant terms, A_n and A'_n. It is assumed that these are both expressed in terms of A'_1. Shortly, it will be clear that this is always the case. The solid has four constants: A_{n+1}, A'_{n+1}, B_{n+1}, and B'_{n+1}. There are three equations, then, and five constants to be determined. A'_{n+1}, B_{n+1}, and B'_{n+1} are found in terms of A_{n+1} and A'_1.

The equation for continuity of normal stress (equation A1a) can be written explicitly as:

$$D_{n+1_{11}}A_{n+1} + D_{n+1_{12}}A'_{n+1} + D_{n+1_{13}}B_{n+1} + D_{n+1_{14}}B'_{n+1} = D_{n_{11}}A_n + D_{n_{12}}A'_n \tag{A2}$$

where, A_n and A'_n are both in terms of A'_1:

$$A_n = a_0 A'_1$$

$$A'_n = a_1 A'_1$$

a_i are constants. Substituting into equation (A2) yields:

$$D_{n+1_{11}}A_{n+1} + D_{n+1_{12}}A'_{n+1} + D_{n+1_{13}}B_{n+1} + D_{n+1_{14}}B'_{n+1} = (D_{n_{11}}a_0 + D_{n_{12}}a_1)A'_1 \tag{A3}$$

In a similar manner, the continuity of normal stress (equation A1b) can be written:

$$D_{n+1_{31}}A_{n+1} + D_{n+1_{32}}A'_{n+1} + D_{n+1_{33}}B_{n+1} + D_{n+1_{34}}B'_{n+1} = (D_{n_{11}}a_0 + D_{n_{12}}a_1)A'_1 \tag{A4}$$

and zero tangential stress at the boundary (equation A1c) can be written as:

$$D_{n+1_{41}}A_{n+1} + D_{n+1_{42}}A'_{n+1} + D_{n+1_{43}}B_{n+1} + D_{n+1_{44}}B'_{n+1} = 0 \tag{A5}$$

A set of constants c_i is defined to simplify notation. Let:

$$c_0 = D_{n_{11}}\alpha_0 + D_{n_{12}}\alpha_1$$

$$c_1 = D_{n_{31}}\alpha_0 + D_{n_{32}}\alpha_1$$

A'_{n+1} can be eliminated from equations (A3) and (A5). This yields:

$$c_2 A_{n+1} + c_3 B_{n+1} + c_4 B'_{n+1} = c_0 A'_1 \tag{A6}$$

where:

$$c_2 = D_{n+1_{11}} - \frac{D_{n+1_{12}} D_{n+1_{41}}}{D_{n+1_{42}}}$$

$$c_3 = D_{n+1_{13}} - \frac{D_{n+1_{12}} D_{n+1_{43}}}{D_{n+1_{42}}}$$

$$c_4 = D_{n+1_{14}} - \frac{D_{n+1_{12}} D_{n+1_{44}}}{D_{n+1_{42}}}$$

Similarly, A'_{n+1} can also be eliminated from equations (A4) and (A5) to give:

$$c_5 A_{n+1} + c_6 B_{n+1} + c_7 B'_{n+1} = c_1 A'_1 \tag{A7}$$

where:

$$c_5 = D_{n+1_{31}} - \frac{D_{n+1_{32}} D_{n+1_{41}}}{D_{n+1_{42}}}$$

$$c_6 = D_{n+1_{33}} - \frac{D_{n+1_{32}} D_{n+1_{43}}}{D_{n+1_{42}}}$$

$$c_7 = D_{n+1_{34}} - \frac{D_{n+1_{32}} D_{n+1_{44}}}{D_{n+1_{42}}}$$

B_{n+1} can now be eliminated from (A6) and (A7) to give and expression for B'_{n+1} in terms of A_{n+1} and A'_1:

$$B'_{n+1} = c_8 A_{n+1} + c_9 A'_1 \tag{A8}$$

where:

$$c_8 = \frac{\dfrac{c_3 c_5}{c_6} - c_2}{c_4 - \dfrac{c_3 c_7}{c_6}}$$

$$c_9 = \frac{c_0 - \dfrac{c_3 c_1}{c_8}}{c_4 - \dfrac{c_3 c_7}{c_8}}$$

Substituting equation (A8) into equation (A7):

$$c_5 A_{n+1} + c_6 B_{n+1} + c_7(c_8 A_{n+1} + c_9 A'_{n+1}) = c_1 A'_1$$

Solving for B_{n+1} yields:

$$B_{n+1} = c_{10} A_{n+1} + c_{11} A'_{n+1} \tag{A9}$$

where:

$$c_{10} = \frac{-c_5 - c_7 c_8}{c_8}$$

$$c_{11} = \frac{c_1 - c_7 c_9}{c_8}$$

Substituting equation (A8) and equation (A9) into equation (A6) yields:

$$D_{n+1_{41}} A_{n+1} + D_{n+1_{42}} + D_{n+1_{43}}(c_{10} A_{n+1} + c_{11} A'_1) + D_{n+1_{44}}(c_8 A_{n+1} + c_9 A'_1) = 0$$

Which can be solved to find and expression for A'_{n+1} in terms of A_{n+1} and A'_1:

$$A'_{n+1} = c_{12} A_{n+1} + c_{13} A'_1 \tag{A10}$$

where:

$$c_{12} = \frac{-D_{n+1_{41}} - D_{n+1_{43}} c_{10} - D_{n+1_{44}} c_8}{D_{n+1_{42}}}$$

$$c_{13} = \frac{-D_{n+1_{43}} c_{11} - D_{n+1_{44}} c_9}{D_{n+1_{42}}}$$

Equations (A10), (A9), and (A8) then give A'_{n+1}, B_{n+1}, and B'_{n+1} in terms of A'_1 and A_{n+1}.

Solid-Fluid Boundary

The solid, layer n, has constants A_n, A'_n, B_n, and B'_n, all expressed in terms of A'_1 and A_n (or A from some inner solid layer). The fluid, layer $n+1$, has constants A_{n+1} and A'_{n+1}. The boundary conditions are the same as in the previous case of a solid-fluid boundary. A_n and A'_n are determined in terms of A'_1. The continuity of radial displacement is written as:

$$D_{n+1_{11}} A_{n+1} + D_{n+1_{12}} A'_{n+1} = c_{16} A_n + c_{17} A'_1 \tag{A11}$$

where:

$$c_{16} = D_{n_{11}}c_{14} + D_{n_{12}}c_{12} + D_{n_{13}}c_{10} + D_{n_{14}}c_8$$

$$c_{17} = D_{n_{11}}c_{15} + D_{n_{12}}c_{13} + D_{n_{13}}c_{11} + D_{n_{14}}c_9$$

The continuity of radial stress gives:

$$D_{n+1_{31}}A_{n+1} + D_{n+1_{32}}A'_{n+1} = c_{18}A_n + c_{19}A'_1 \tag{A12}$$

where:

$$c_{18} = D_{n_{31}}c_{14} + D_{n_{32}}c_{12} + D_{n_{33}}c_{10} + D_{n_{34}}c_8$$

$$c_{19} = D_{n_{31}}c_{15} + D_{n_{32}}c_{13} + D_{n_{33}}c_{11} + D_{n_{34}}c_9$$

The condition that the axial stress must vanish at the interface is written explicitly as:

$$0 = c_{20}A_n + c_{21}A'_1 \tag{A13}$$

where:

$$c_{20} = D_{n_{41}}c_{14} + D_{n_{42}}c_{12} + D_{n_{33}}c_{10} + D_{n_{34}}c_8$$

$$c_{21} = D_{n_{41}}c_{15} + D_{n_{42}}c_{13} + D_{n_{43}}c_{11} + D_{n_{44}}c_9$$

A_n is eliminated from equation (A11) and (A13). The result is:

$$D_{n+1_{11}}A_{n+1} + D_{n+1_{12}}A'_{n+1} = c_{22}A'_1 \tag{A14}$$

where:

$$c_{22} = c_{17} - \frac{c_{18}c_{21}}{c_{20}}$$

Similarly eliminating A_n from equations (A12) and (A13) yields:

$$D_{n+1_{31}}A_{n+1} + D_{n+1_{32}}A'_{n+1} = c_{23}A'_1 \tag{A15}$$

where:

$$c_{23} = c_{19} - \frac{c_{18}c_{21}}{c_{20}}$$

A'_{n+1} is then eliminated from equations (A14) and (A15). The result is:

$$A_{n+1} = a_0 A'_1 \tag{A16}$$

where:

$$a_0 = \frac{c_{17} - \dfrac{c_{18}c_{21}}{c_{20}} - \left(c_{19} - \dfrac{c_{18}c_{21}}{c_{20}}\right)\left[\dfrac{D_{n+1_{12}}}{D_{n+1_{32}}}\right]}{D_{n+1_{11}} - \dfrac{D_{n+1_{12}}D_{n+1_{31}}}{D_{n+1_{32}}}}$$

Substituting equation (A16) into equation (A14) yields:

$$A'_{n+1} = a_1 A'_1 \tag{A17}$$

where:

$$a_1 = \frac{c_{22} - D_{n+1_{11}} a_0}{D_{n+1_{12}}}$$

If this fluid layer is the outermost fluid layer, (layer f), the displacements and stresses are now related across all the layers. Otherwise, the results of this solid-fluid case can serve as input for the fluid-solid boundary conditions if the next layer $n+2$ is a solid. (Recall that the constants a_0 and a_1 were used earlier in the case of a fluid-solid boundary.)

Solid-Solid Boundary

In the inner solid n, there are four constants A_n, A'_n, B_n, and B'_n, all of which are expressed in terms of A_n and A'_1. The outer solid has constants A_{n+1}, A'_{n+1}, B_{n+1}, and B'_{n+1}. The boundary conditions at r_n are the continuity of radial and axial displacements and stresses:

$$u_n(r_n) = u_{n+1}(r_n) \tag{A18a}$$

$$v_n(r_n) = v_{n+1}(r_n) \tag{A18b}$$

$$\sigma_n(r_n) = \sigma_{n+1}(r_n) \tag{A18c}$$

$$\tau_n(r_n) = \tau_{n+1}(r_n) \tag{A18d}$$

A_{n+1}, A'_{n+1}, B_{n+1}, and B'_{n+1} will be found in terms of A'_1 and A_n.

If there are several solid layers together in a group, this section is used repeatedly, determining all constants in terms of A'_1 and A_i, where i is the innermost layer of the group. All four components of the displacement-stress vector are continuous across r_n, the interface between the two solid layers n and $n+1$. Thus:

$$\mathbf{u}_n(r_n) = \mathbf{u}_{n+1}(r_n)$$

or

$$\mathbf{D}_n(r_n)\mathbf{a}_n = \mathbf{D}_{n+1}(r_n)\mathbf{a}_{n+1}$$

Rearranging:

$$\mathbf{a}_{n+1} = \mathbf{D}_{n+1}^{-1}(r_n)\mathbf{D}_n(r_n)\mathbf{a}_n \tag{A19}$$

$\mathbf{a}_n$ is known in terms of A'_1 and A_n, (or A from some inner solid layer). Equation (A19) can thus be written:

$$\begin{bmatrix} A_{n+1} \\ A'_{n+1} \\ B_{n+1} \\ B'_{n+1} \end{bmatrix} = \mathbf{D}_{n+1}^{-1}(r_n)\mathbf{D}_n(r_n) \begin{bmatrix} c_{14}A_n + c_{15}A'_1 \\ c_{12}A_n + c_{13}A'_1 \\ c_{10}A_n + c_{11}A'_1 \\ c_8 A_n + c_9 A'_1 \end{bmatrix} \tag{A20}$$

Equation (A20) gives A_{n+1}, A'_{n+1}, B_{n+1}, and B'_{n+1} in terms of A_n and A'_1. The results can be put into the form:

$$A_{n+1} = c_{14}A_n + c_{15}A'_1$$

$$A'_{n+1} = c_{12}A_n + c_{13}A'_1$$

$$B_{n+1} = c_{10}A_n + c_{11}A'_1$$

$$B'_{n+1} = c_8 A_n + c_9 A'_1$$

where the constants c_i do *not* have the same values as in equation (A20). They are new values determined by the matrix multiplication. The reason for using the same terms is that if the next layer $(n+2)$ is also solid, these new values are substituted directly into equation (A20) to continue through all solid layers.

Fluid-Fluid Boundary

The inner fluid, layer n, has constants A_n and A'_n, both in terms of A'_1. The outer fluid has constants A_{n+1} and A'_{n+1}. The boundary conditions are the continuity of radial displacement and stress:

$$u_n(r_n) = u_{n+1}(r_n) \tag{A21a}$$

$$\sigma_n(r_n) = \sigma_{n+1}(r_n) \tag{A21b}$$

The inner fluid has constants A_n and A'_n which are both known in terms of A'_1. The outer fluid has constants A_{n+1} and A'_{n+1}.

The continuity of radial displacement (equation A21a) can be written explicitly as:

$$A'_1(a_0 \mathbf{D}_{n_{11}} + a_1 \mathbf{D}_{n_{12}}) = \mathbf{D}_{n+1_{11}}A_{n+1} + \mathbf{D}_{n+1_{32}}A'_{n+1} \tag{A22}$$

The continuity of radial stress (equation A21b) is:

$$A'_1(a_0 \mathbf{D}_{n_{31}} + a_1 \mathbf{D}_{n_{32}}) = \mathbf{D}_{n+1_{31}}A_{n+1} + \mathbf{D}_{n+1_{32}}A'_{n+1} \tag{A23}$$

A'_{n+1} is eliminated from equations (A22) and (A23) to yield:

$$A_{n+1} = a'_0 A'_1 \tag{A24}$$

where

$$a'_0 = \frac{a_0 D_{n_{11}} + a_1 D_{n_{12}} - \dfrac{D_{n+1_{12}}}{D_{n+1_{32}}}(a_0 D_{n_{31}} + a_1 D_{n_{32}})}{D_{n+1_{11}} - \dfrac{D_{n+1_{12}} D_{n+1_{31}}}{D_{n+1_{32}}}} \tag{A25}$$

A'_{n+1} is determined by substituting equation (A24) into equation (A22). The result is:

$$A'_{n+1} = a'_1 A'_1 \tag{A26}$$

where:

$$a'_1 = \frac{a_0 D_{n_{11}} + a_1 D_{n_{12}} - a'_0 D_{n+1_{11}}}{D_{n+1_{12}}} \tag{A27}$$

a'_0 and a'_1 replace a_0 and a_1 if further calculations are required.

FLUID) SOLID AND/OR FLUID LAYERS) FLUID LAYER f) SOLID LAYERS) SOLID
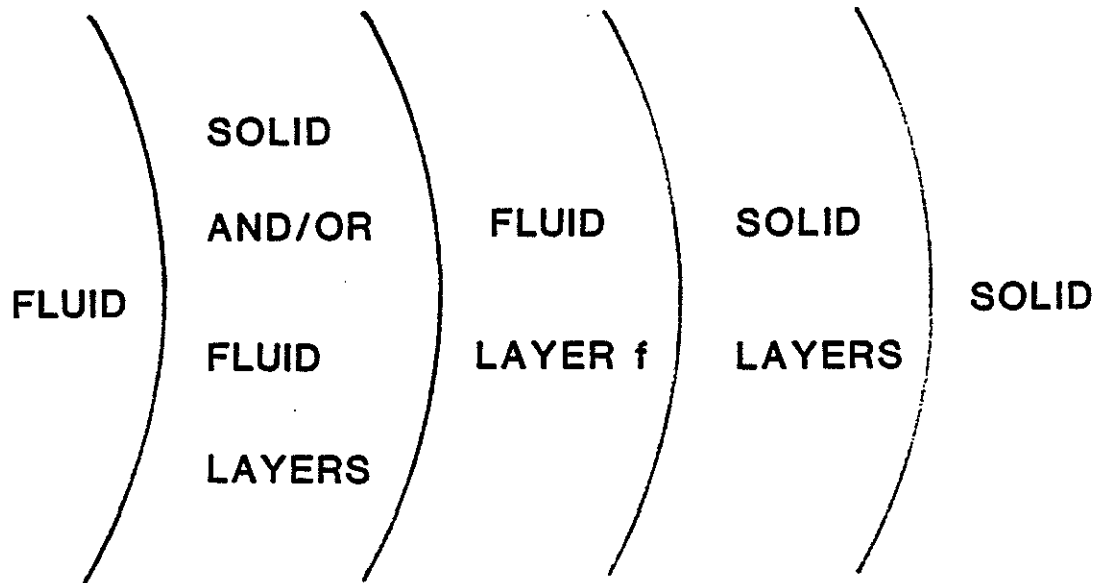
Fig. 1. Geometry of the model. The first layer, the central fluid cylinder, is fluid. The outer, infinite layer is solid. The intermediate layers can be either solid or fluid. The outermost fluid layer is labeled layer f.
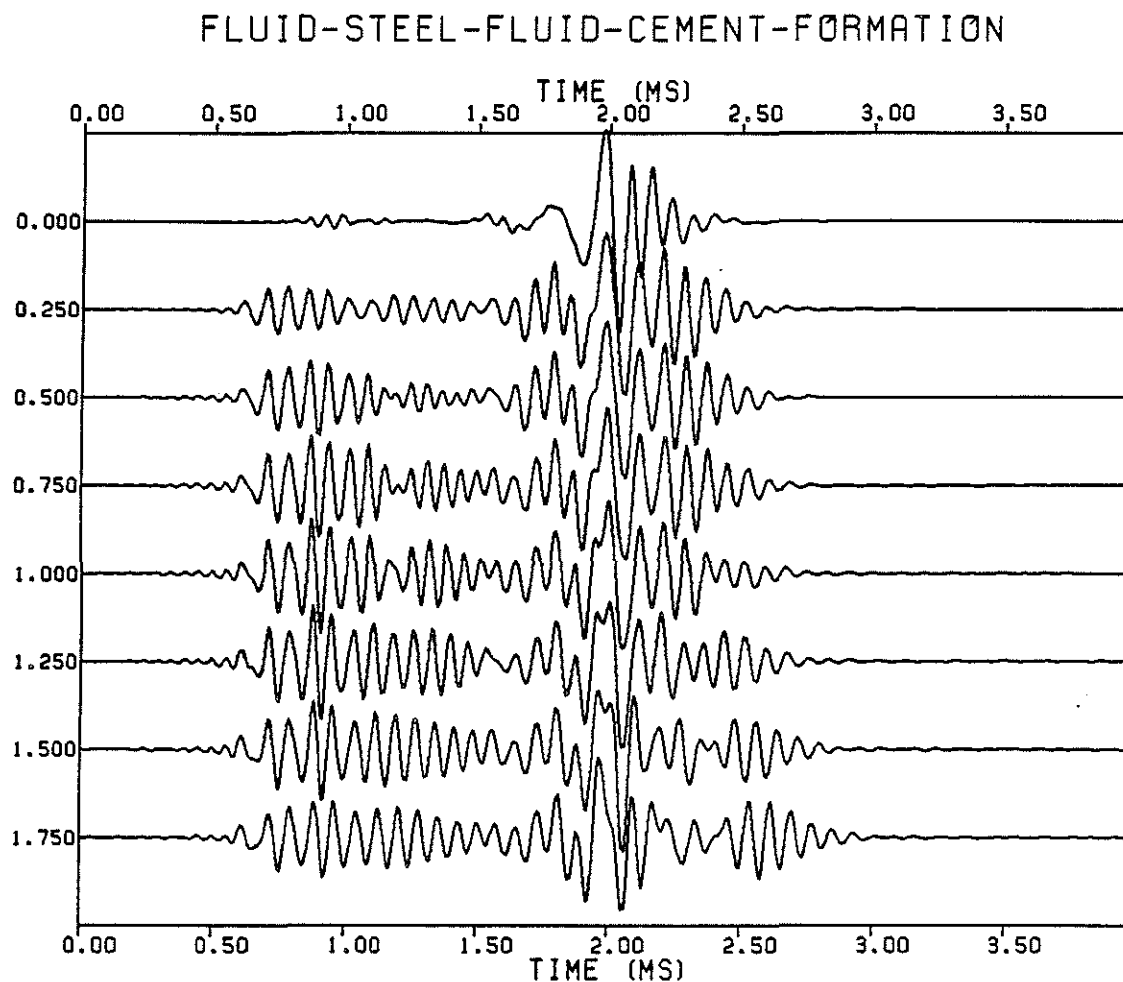
FLUID-STEEL-FLUID-CEMENT-FORMATION

Fig. 2. Microseismograms for various thicknesses of the fluid layer between the steel and the cement. This is the free pipe situation. The source-receiver separation is 10 ft. The source center frequency is 13 kHz. The fluid layer thickness increases in .25 inch increments. The cement layer thickness decreases by this amount. The first microseismogram has no fluid layer (the well bonded case) and the last has no cement layer. The P velocity of the formation is 13.12 ft/ms and the S velocity is 7.0 ft/ms.

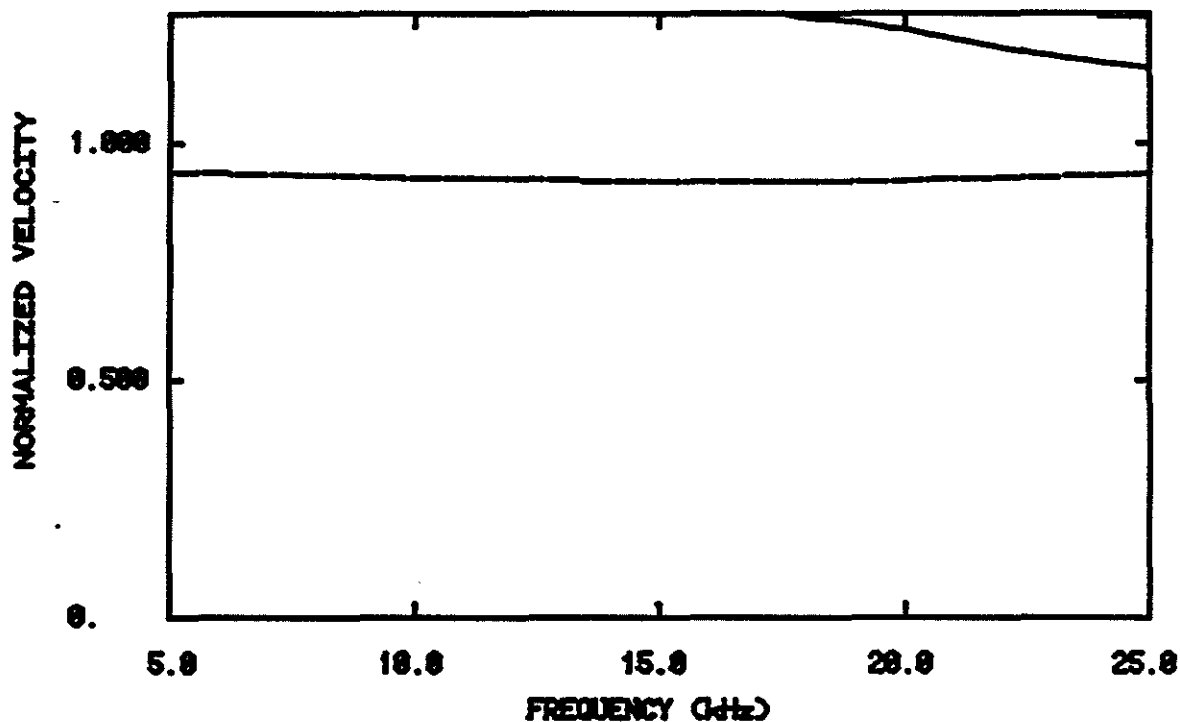| r	Vp	Vs	rho
0.154167	5.500	0.	1.200
0.167500	20.000	11.000	7.500
0.333333	9.250	5.570	1.920
0.	13.120	7.000	2.100

Fig. 3. Phase velocity dispersion curves for the well bonded situation. The velocities are normalized to the borehole fluid velocity. The Stoneley mode (dashed line) and two modes of the pseudo-Rayleigh (solid lines) are present in this frequency range.

Tubman et al.

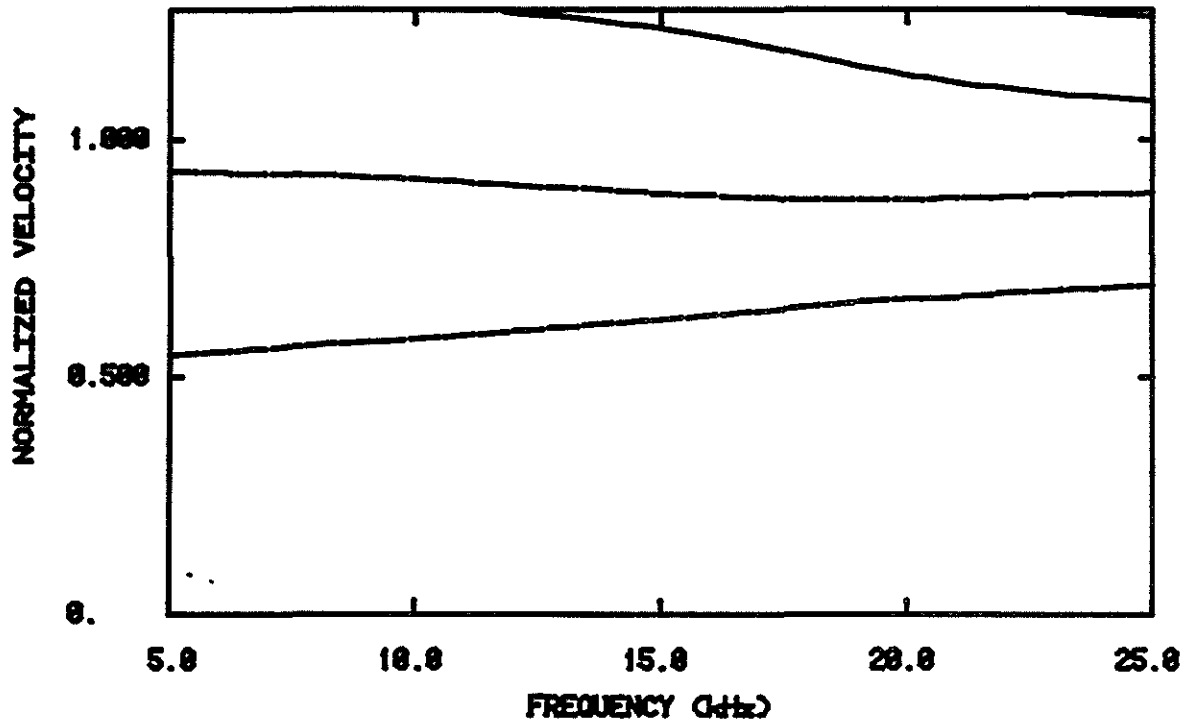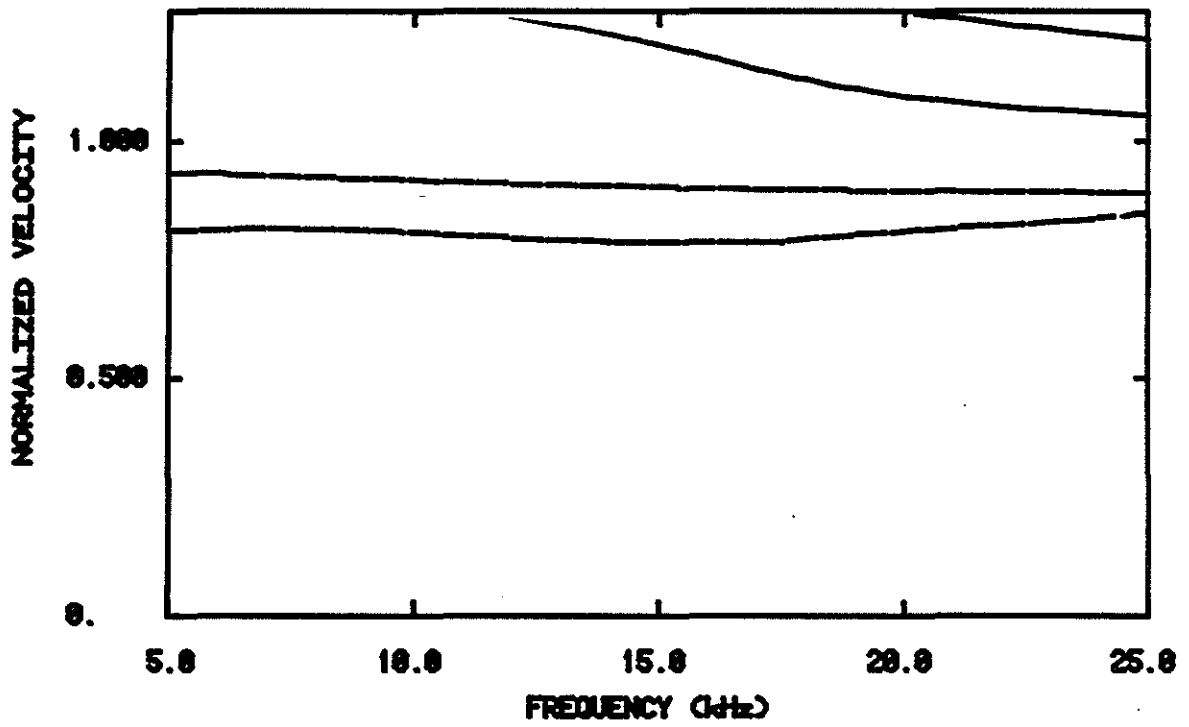| r	Vp	Vs	rho
0.154167	5.500	0.	1.200
0.187500	20.000	11.000	7.500
0.208333	5.500	0.	1.200
0.333333	9.250	5.070	1.920
0.	13.120	7.000	2.100

Fig. 4. Phase velocity dispersion curves for the free pipe situation where the fluid layer between the steel and the cement is .25 inches.

r	Vp	Vs	rho
0.154167	5.500	0.	1.200
0.187500	20.000	11.000	7.500
0.312500	5.500	0.	1.200
0.333333	9.250	5.670	1.920
0.	13.120	7.000	2.100

Fig. 5. Phase velocity dispersion curves for the free pipe situation where the fluid layer between the steel and the cement is 1.5 inches.

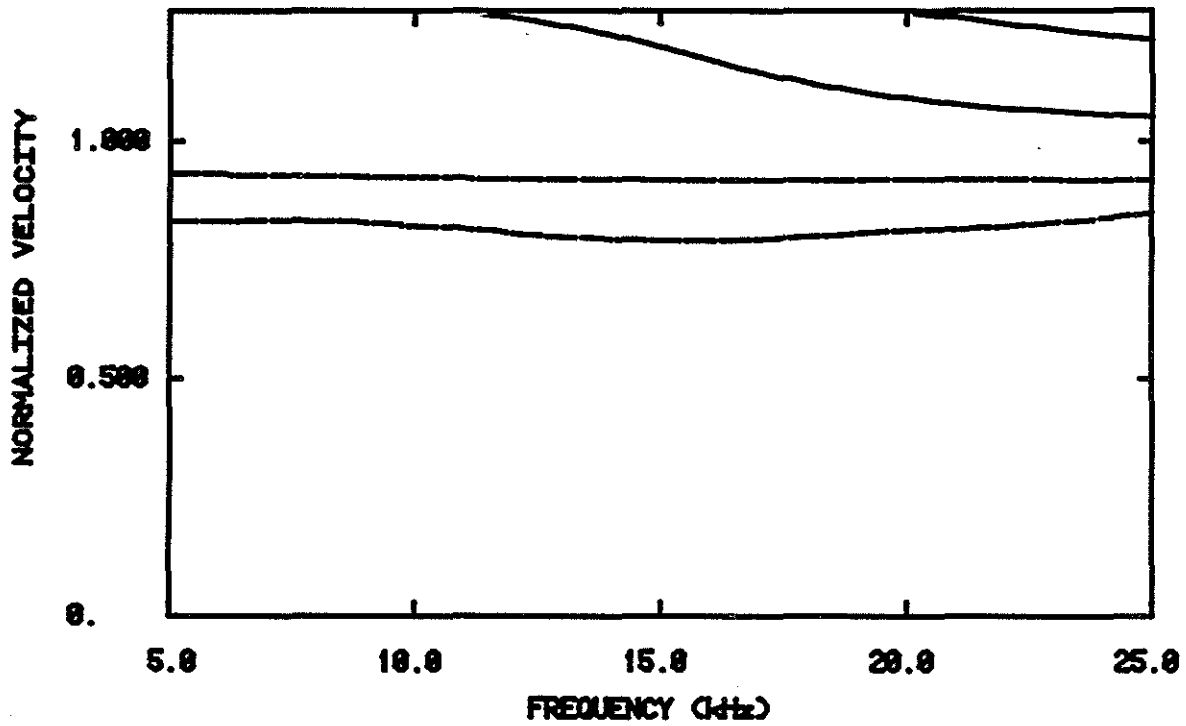| r	Vp	Vs	rho
0.154167	5.500	0.	1.200
0.187500	20.000	11.000	7.500
0.333333	5.500	0.	1.200
0.	13.120	7.000	2.100

Fig. 6. Phase velocity dispersion curves for the free pipe situation. There is no cement layer between the steel and the formation.

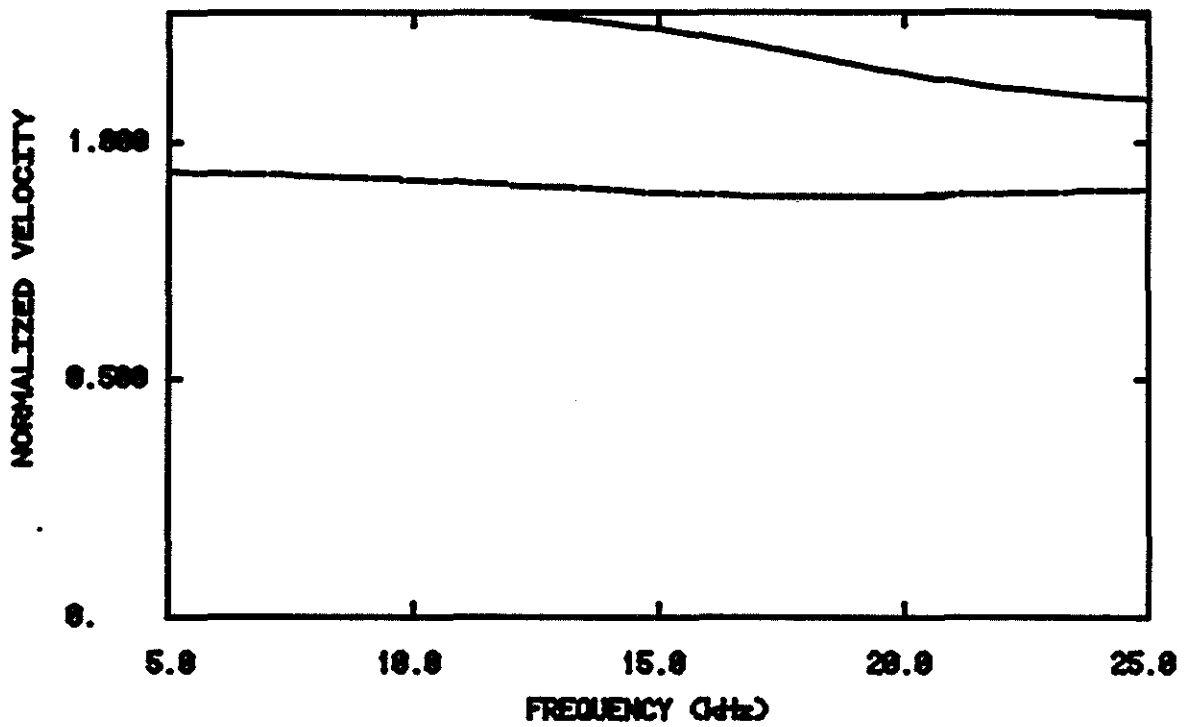| r	Vp	Vs	rho
0.154167	5.500	0.	1.200
0.187500	20.000	11.000	7.500
0.187583	5.500	0.	1.200
0.333333	9.250	5.570	1.920
0.	13.120	7.000	2.100

Fig. 7. Phase velocity dispersion curves for the case of a microannulus. The thickness of the fluid layer between the steel and the cement is .001 inches.
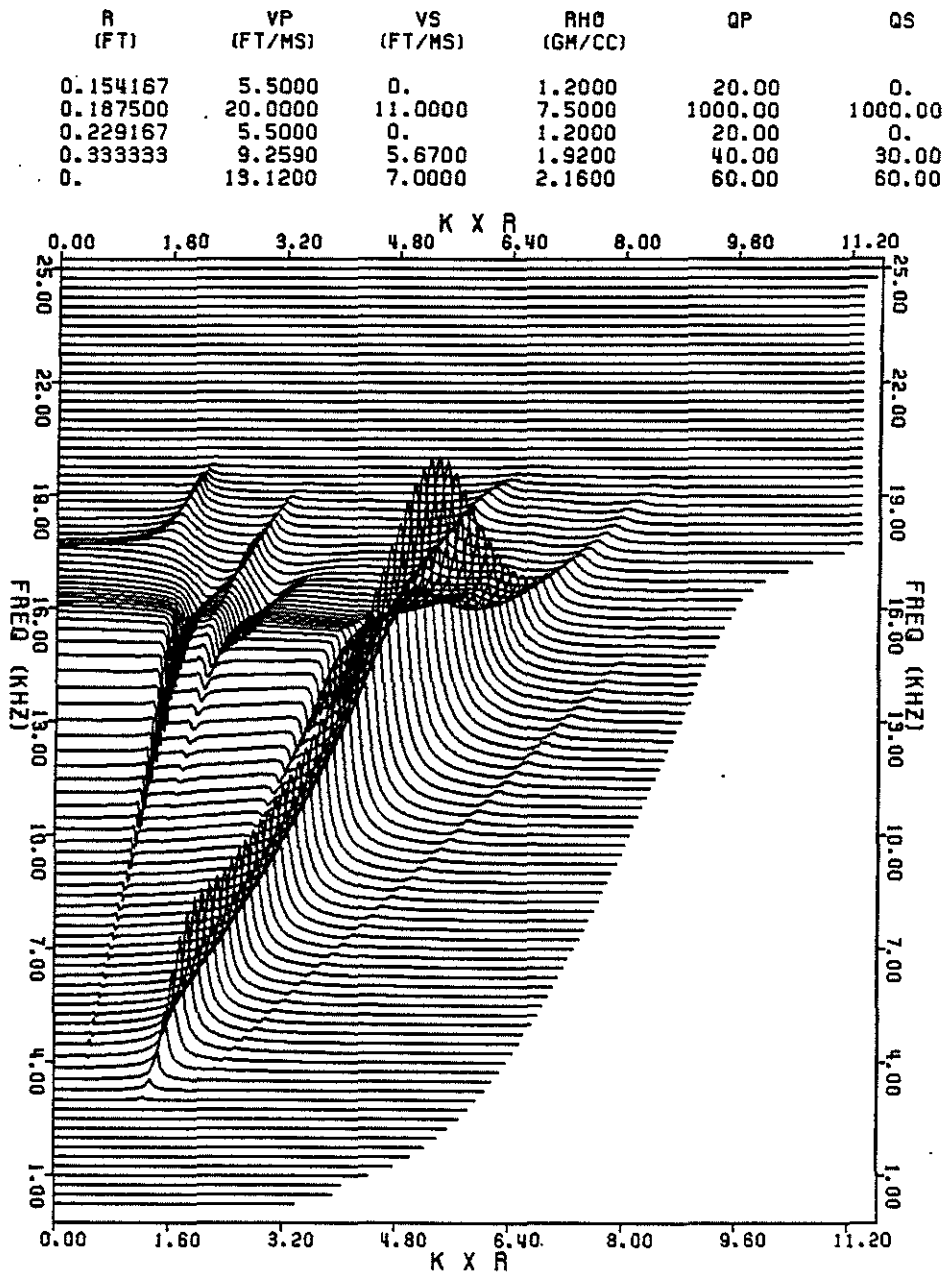
Tubman et al.

R (FT)	VP (FT/MS)	VS (FT/MS)	RHO (GM/CC)	QP	QS
0.154167	5.5000	0.	1.2000	20.00	0.
0.187500	20.0000	11.0000	7.5000	1000.00	1000.00
0.229167	5.5000	0.	1.2000	20.00	0.
0.333333	9.2590	5.6700	1.9200	40.00	30.00
0.	13.1200	7.0000	2.1600	60.00	60.00

Fig. 8. Magnitude of the frequency-wavenumber spectrum for a free pipe situation. The spectrum has been multiplied by the source function. The fluid layer between the steel and the cement has a thickness of .5 inches.

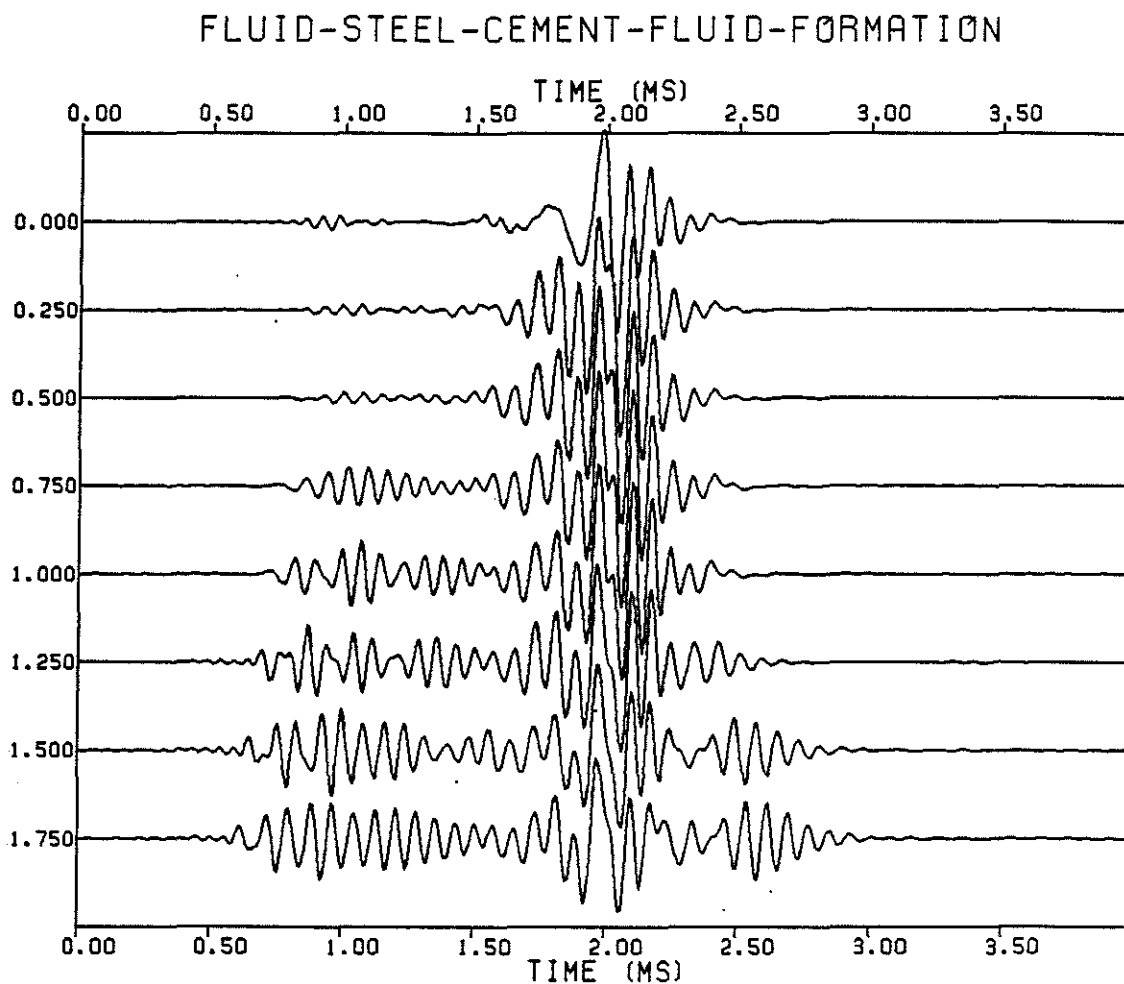FLUID-STEEL-CEMENT-FLUID-FORMATION

Fig. 9. Microseismograms for various thicknesses of the fluid layer between the cement and the formation. The fluid layer thickness increases in .25 inch increments. The cement layer thickness decreases by this amount. The first microseismogram has no fluid layer (the well bonded case) and the last has no cement layer. The P velocity of the formation is 13.12 ft/ms and the S velocity is 7.0 ft/ms.
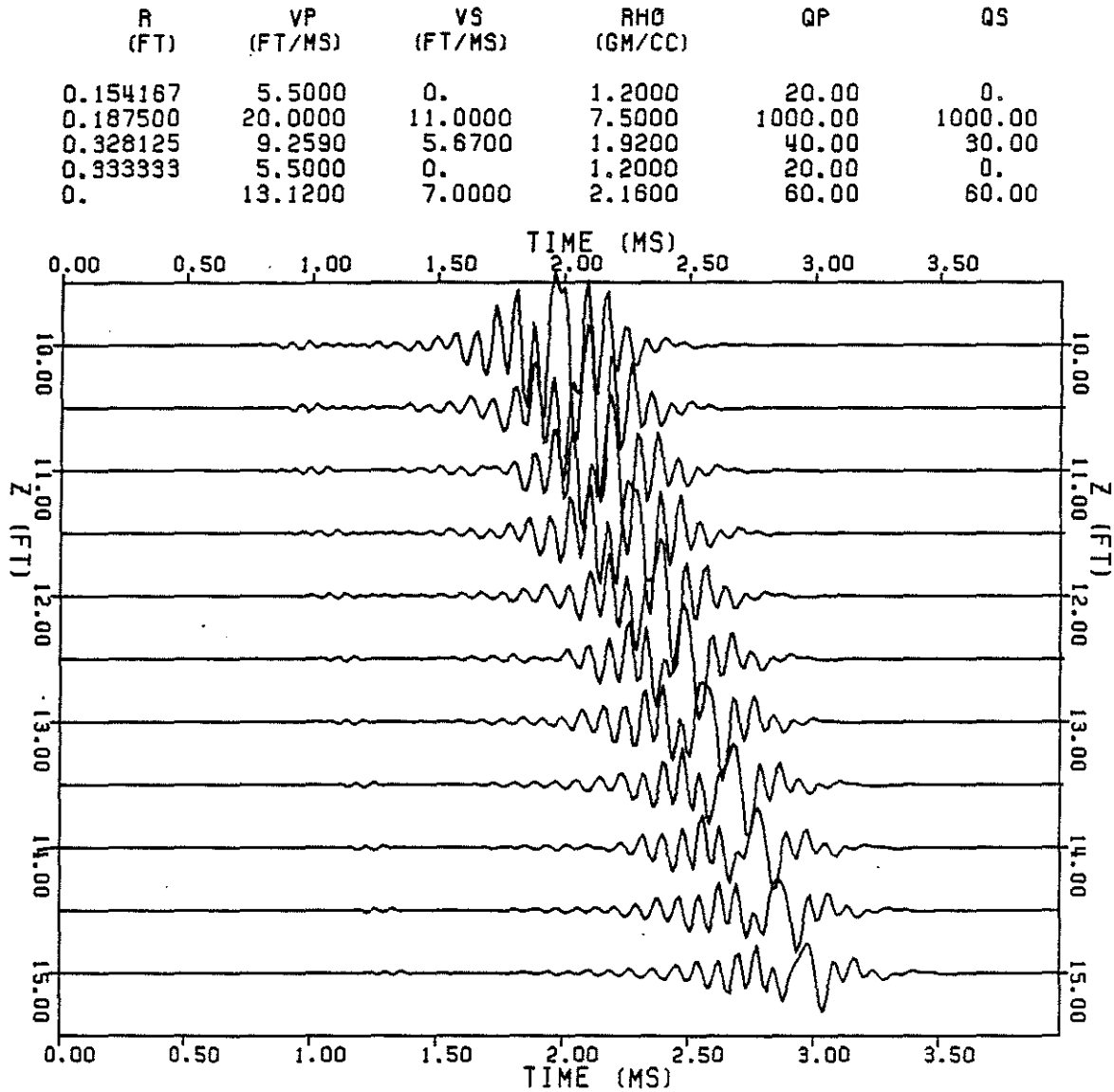
| R (FT)	VP (FT/MS)	VS (FT/MS)	RHO (GM/CC)	QP	QS
0.154167	5.5000	0.	1.2000	20.00	0.
0.187500	20.0000	11.0000	7.5000	1000.00	1000.00
0.328125	9.2590	5.6700	1.9200	40.00	30.00
0.333333	5.5000	0.	1.2000	20.00	0.
0.	13.1200	7.0000	2.1600	60.00	60.00

Fig. 10. Microseismograms for a case of good steel-cement bond but no cement-formation bond. The cement thickness is 1.6875 inches and the fluid thickness is.0625.

R (FT)	VP (FT/MS)	VS (FT/MS)	RHO (GM/CC)	QP	QS
0.154167	5.5000	0.	1.2000	20.00	0.
0.187500	20.0000	11.0000	7.5000	1000.00	1000.00
0.328125	9.2590	5.6700	1.9200	40.00	30.00
0.432267	5.5000	0.	1.2000	20.00	0.
0.	13.1200	7.0000	2.1600	60.00	60.00
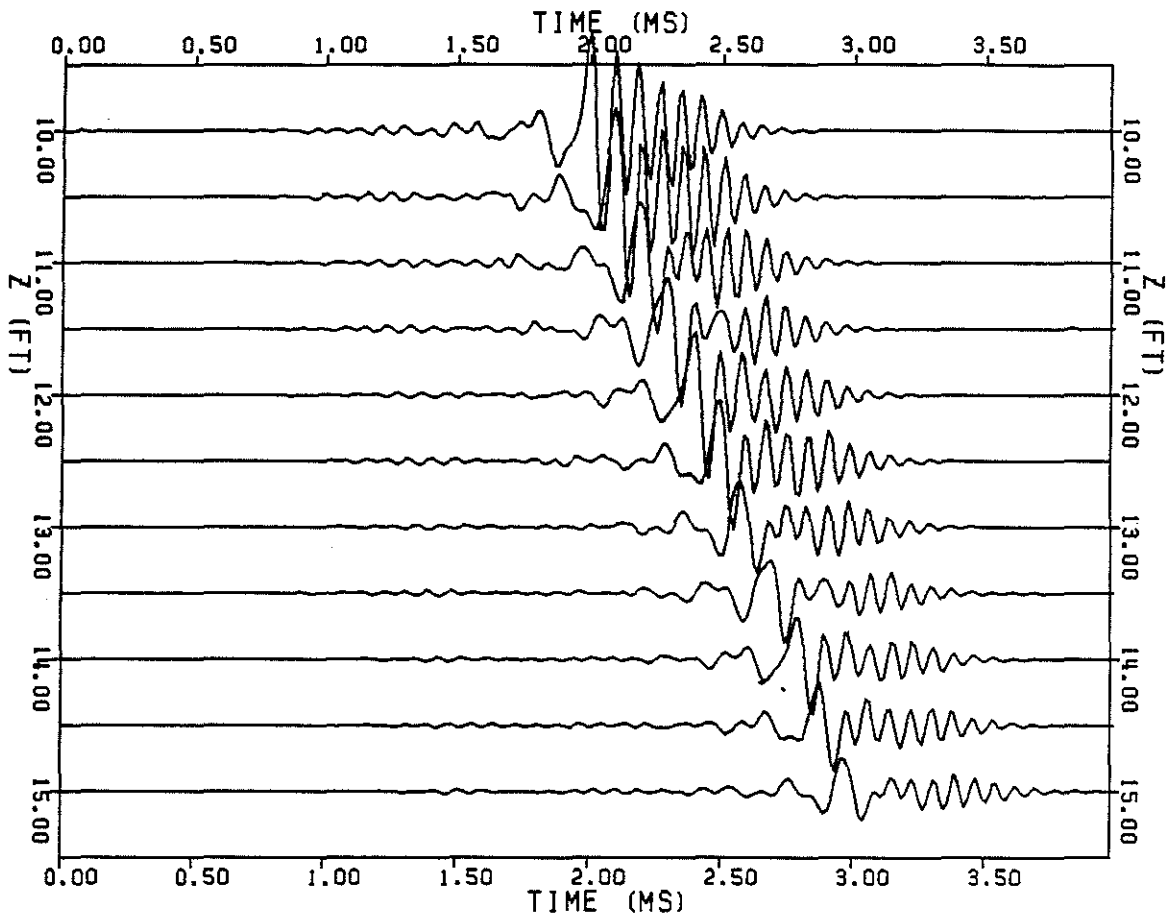
Fig. 11. Microseismograms for a case of good steel-cement bond but no cement-formation bond. The cement thickness is the same as in Figure 10, but here the hole radius is larger so the fluid layer between the cement and the formation has a thickness of 1.25 inches.

Tubman et al.

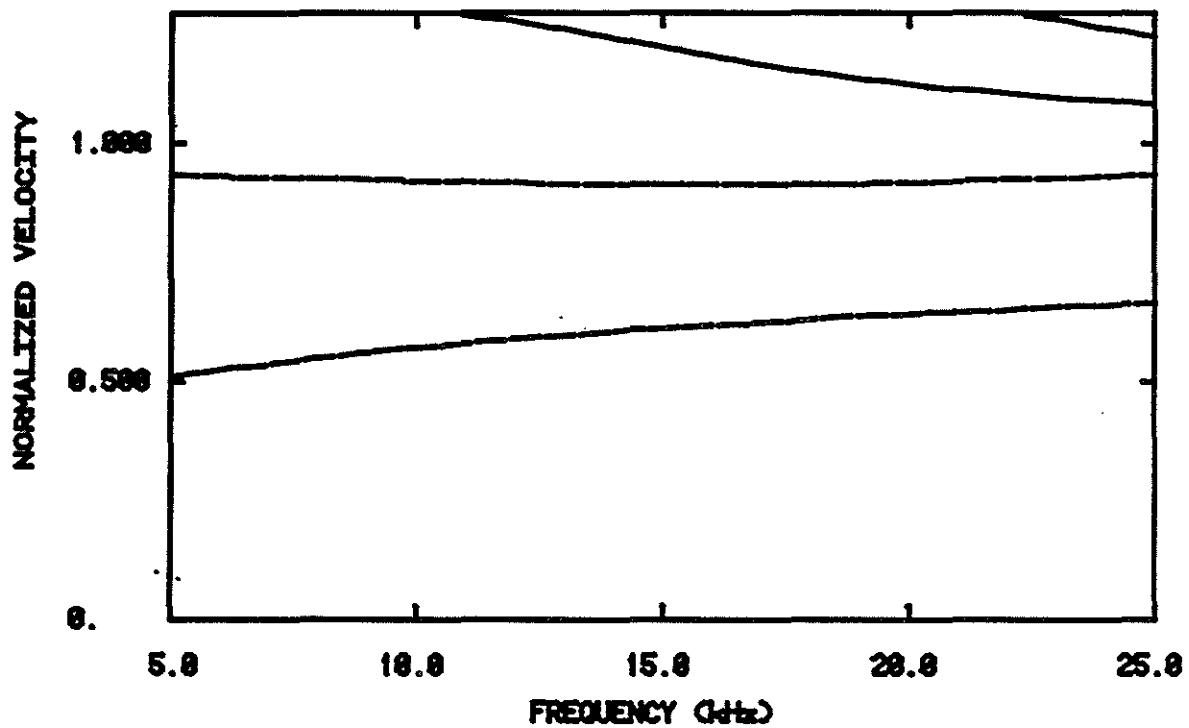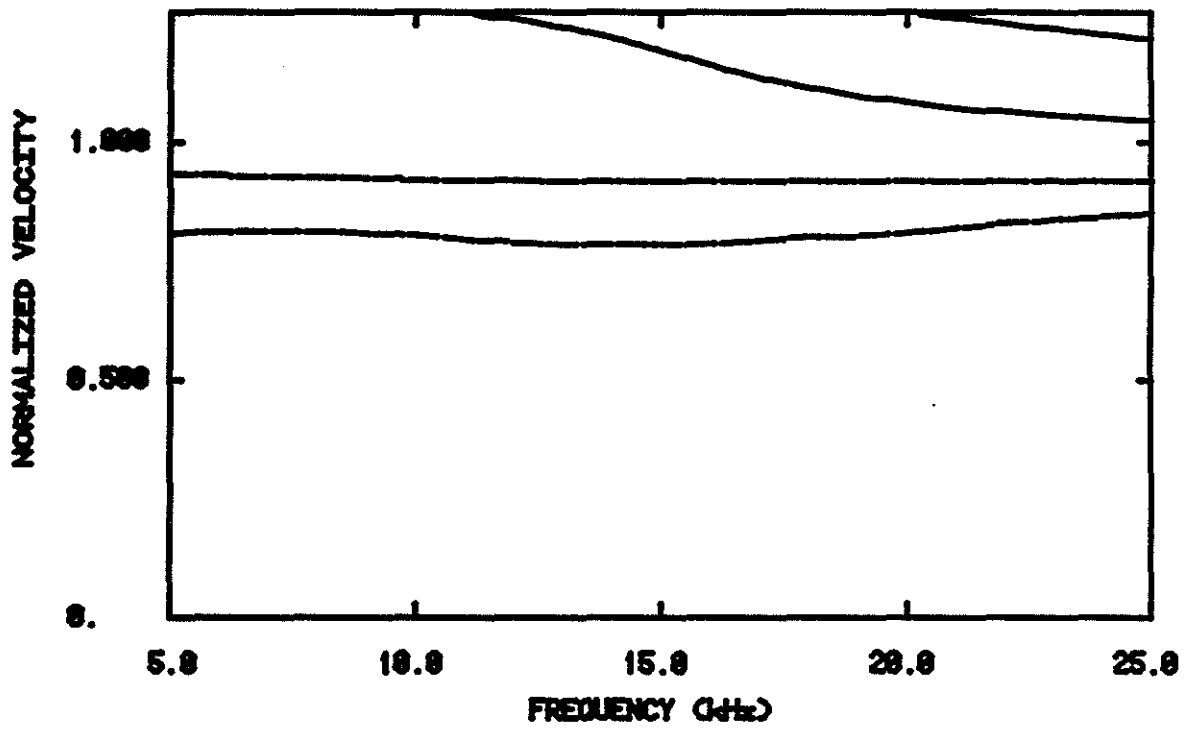| r	Vp	Vs	rho
0.154167	5.500	0.	1.200
0.187500	20.000	11.000	7.500
0.312500	9.250	5.670	1.920
0.333333	5.500	0.	1.200
0.	13.120	7.000	2.100

Fig. 12. Phase velocity dispersion curves for the case of good steel-cement bond but no cement-formation bond. The fluid layer thickness is .25 inches.

Unbonded Cased Holes

r	Vp	Vs	rho
0.154167	5.500	0.	1.200
0.187500	20.000	11.000	7.500
0.208333	9.250	5.670	1.920
0.333333	5.500	0.	1.200
0.	13.120	7.000	2.100

Fig. 13. Phase velocity dispersion curves for the case of good steel-cement bond but no cement-formation bond. The fluid layer thickness is 1.5 inches.

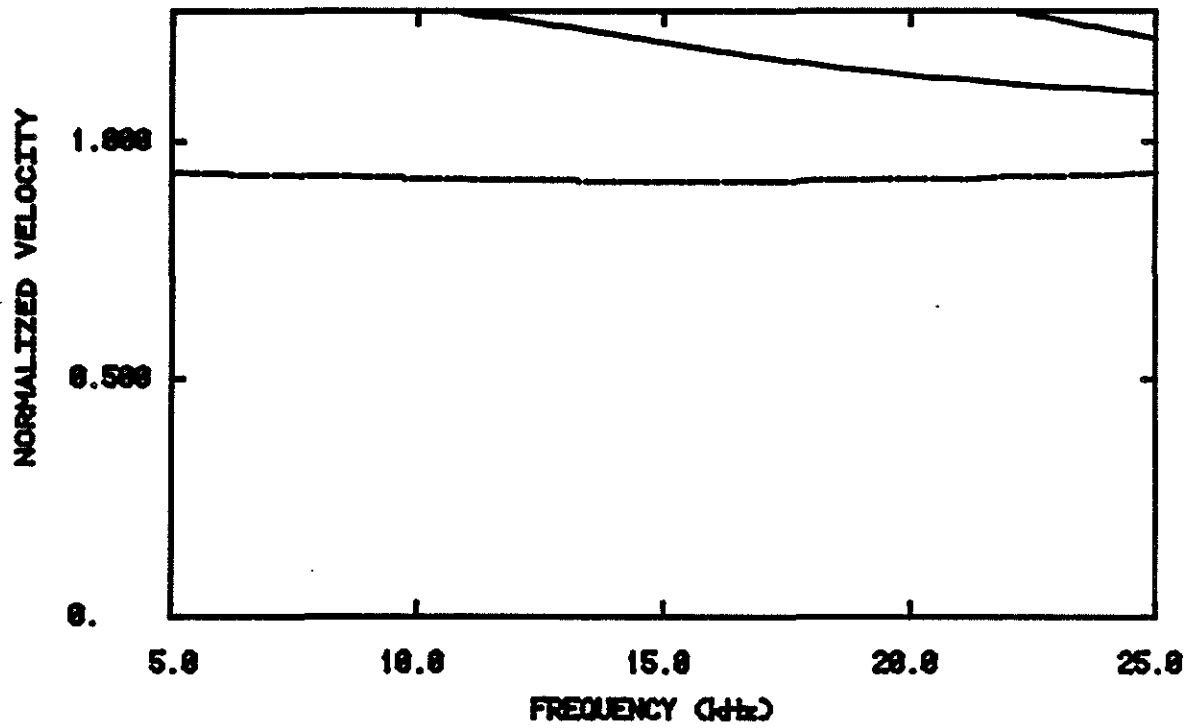| r	Vp	Vs	rho
0.154167	5.500	0.	1.200
0.187500	20.000	11.000	7.500
0.333250	9.250	5.070	1.920
0.333333	5.500	0.	1.200
0.	13.120	7.000	2.100

Fig. 14. Phase velocity dispersion curves for a very thin (.001 inch) fluid layer between the cement and the formation.